Geophys. J. R. astr. Soc. (1983) 74, 787–808

Descriptive statistical model of earthquake source radiation and its application to an estimation of short-period strong motion

A. A. Gusev *Institute of Volcanology, Petropavlovsk-Kamchatsky 683 006, USSR*

Received 1983 January 6; in original form 1982 March 9

Summary. A wide-band source spectrum scaling law is derived from various data sources; its main features are: a lack of similitude and two characteristic frequencies of about 0.2 and 5–10 Hz. An average short-period radiation flux from the source surface does not greatly depend on magnitude; it is about 3×10^7 erg cm^{-2} s and short-period efficiency is about 10 per cent. For sources of great earthquakes a short-period radiation flux is relatively low. The spectrum scaling law is used to determine near-field accelerations. Formulae to estimate 'static' and wavefield accelerations of incoherently radiating sources are derived and applied to calculate the average relation between maximum acceleration and intensity, and distance and magnitude. Theoretical relations agree well with the empirical ones.

Introduction

Description and simulation of elastic wave radiation generated by an earthquake source is a problem of current interest. In particular, its application is important in ground motion prediction during large earthquakes. To solve this problem, a perfect and realistic description of movement inside the source should be proposed. Broadly, this description should be dynamical, starting with the initial elastic and gravitational stress field, distribution of elastic moduli, plasticity and strength parameters. It should also reflect dynamical rupture propagation (interacting with elastic wave stress field) through the non-linear and heterogeneous Earth's medium. The less ambitious and more common approach considers only the kinematics of rupture. In such a case, a realistic model can be chosen, yet the dynamical description is omitted and the whole approach becomes merely phenomenological.

Several source formation models are in frequent use, mainly those of running dislocation step (Haskell 1964) and of growing crack (Kostrov 1964, 1966; Burridge & Halliday 1971). Strictly speaking, the dislocation model is unrealistic because the dislocation step can be neither dynamically (running step) nor statically (step at the perimeter of source area) supported. It was applied, however, with great success to the interpretation of long-period observations. With only several parameters to adjust (length L and sometimes width W of a source, rupture velocity V and dislocation value B) this model is easy to fit, and it evidently describes some gross features of the source process.

The crack model is more realistic and has an important advantage in that it is based on the dynamical treatment of the problem. Yet the analytical approach can be applied only to an infinitely growing crack in an homogeneous medium. Stopping crack can only be treated numerically (Das & Aki 1977a, b). This approach is promising but difficult, therefore the most interesting case of a two-dimensional asymmetrically growing crack has not yet been studied.

When the problem is treated theoretically and then compared with field geological data, some properties of a real source are found to be missing in the theory. The main differences are: (1) curvature and multiplicity of faults (joints), (2) roughness of fault surface, (3) tensile component of fault wall movement (in addition to shear component) in many sections of a fault. A wide class of models of brittle cracks with flat smooth surfaces was analysed by Dahlen (1974), who, after Kostrov (1964), showed that the far-field radiation spectrum of such a source falls off as f^{-3} or steeper at high frequencies, which is in direct contradiction with observational data.

The classical papers of Haskell (1966) and Aki (1967) introduced the stochastic source function to describe the effects of source microstructure, e.g. roughness. The realistic fall-off of spectrum was achieved by the proposal of a suitable source autocovariance function. This approach was developed further by Andrews (1980, 1981). An alternative approach is to put obstacles (barriers) in the way of a crack tip; one-dimensional (Das & Aki 1977a, b) and quasi-two-dimensional (Mikumo & Miyatake 1978) cases were numerically treated, the last one with randomly distributed barriers. The essentially new property of models with barriers is the possibility that the source consists of several kinematically separated patches. Varying the barrier strength, both 'one-patch' movement with temporary stopping or 'several-patches' movement can be simulated. A versatile barrier model obviously describes some essential features of real sources.

We shall develop, however, a model of another kind, which is nevertheless stochastic in nature. But before its introduction we shall demonstrate that any realistic source model must be stochastic.

On paradoxes of deterministic source model

We shall now show that any deterministic source model, on condition of an approximate similitude of sources of different sizes, leads to some rather unrealistic predictions. On condition of similitude, let length L be the only dimensional parameter, then the maximum acceleration on the fault will be scaled

$$a \propto L/T^2 \propto L^{-1} \tag{1}$$

where $T \propto L$ is the characteristic time. Thus the larger the source, the less acceleration should be near the fault. In the far field (distance $r \gg L$), similitude predicts $a \propto L^{-1}$ for scaled distance $r = kL$. Assuming geometrical spreading $a(r) \propto r^{-1}$, we obtain for a given distance r_0:

$$a(r_0) = a(kL) \cdot (kL/r_0) \propto LL^{-1} = \text{constant} \tag{2}$$

for any L. Therefore far field acceleration is independent from the source size.

Let us reproduce the far field result in another way. For displacement and acceleration spectra at a given distance we have

$$\begin{aligned} u(f) &\propto M_0 \\ a(f) \equiv \ddot{u}(f) &\propto M_0 f_0^2 \end{aligned} \tag{3}$$

where $M_0 \propto L^3$ is the source moment, and $f_0 = T^{-1}$. In the deterministic case, we obtain peak acceleration a_p by simply returning to the time domain; an integration by f leads to

$$a_p \propto M_0 f_0^3 \propto L^3 L^{-3} = \text{constant}. \tag{4}$$

In the stochastic case Parseval's theorem should be used instead

$$\overline{a^2(f)}\,\Delta f = \overline{a^2(t)}\,\Delta t,$$

where Δf and Δt are bandwidth and duration, and the dash above means average. Assume $\Delta t \propto T \propto L$ and Δf = constant (this is empirically plausible and roughly true, for example, for ω^{-2} model of Aki with absorption). Then for rms acceleration in the far field we obtain

$$a_{rms} \equiv \left[\overline{a^2(t)}\right]^{1/2} \propto M_0 f_0^{-2.5} \propto L^{0.5}. \tag{5}$$

Peak value a_p increases with L and Δt slightly faster, say, as $L^{0.7}$. This is much more reasonable than a_p = constant and can be compared with the empirical relation $a_p \propto L^{0.9}$. To derive the last expression one should combine three widely used relations for L, a_p, intensity I and magnitude M (*Seismic microzoning* 1977):

$$I = \log_2 a_p + \text{constant}$$

$$I = 1.5M + f(r)$$

$$\log L = 0.5M + \text{constant}.$$

No such straightforward derivation was found for the near field but estimates obtained below predict a very slow growth of a with L, which is in agreement with empirical data.

Therefore stochastic source models are obviously more promising than the deterministic ones in search of a description of the whole radiation spectrum of real earthquake sources.

Conceptual description of stochastic model

We do not intend to construct here a complete and consistent description of a source, including the dynamics, microstructure of a rupture and so on. We shall limit ourselves to a descriptive approach, but even this will lead us to some rather useful implications. However, we shall base our discussion on some physical concepts of the dynamical source.

Bearing this in mind and following the pioneering ideas of Housner (1955), developed independently in papers by Shebalin (1971) and Blandford (1975), we shall introduce a concept of subsource, considering it as a step or element of the main rupturing process. A subsource is characterized by its own size and duration. Radiation pulse generated by a subsource is supposed to be 'smooth', with a displacement spectrum of f^{-3} or steeper. Physically subsources can correspond to: rupture bifurcation, en-echelon propagation and secondary rupture formation; local and temporal fault wall interlocking or high friction patches; jerks of crack tip movement on barriers. All these kinds of subsources are of shear type. Tensile subsources (Haskell 1964; Blandford 1975) exist as well. They are generated by waviness and bumps on fault walls (Aki 1972), bends and kinks of fault trace, or by a pressure jump associated with friction heating in a wet environment (Sibson 1977). The subsource size roughly corresponds to the inter-barrier distance or to patch size in the barrier model. However, we postulate that subsources of different types and sizes can overlap in space and time; see Boatwright (1982) and Papageorgio & Aki (1982) for models with non-overlapping subsources. Subsources are situated within the limits of main rupture and emerge during its growth. From this point of view aftershocks may be considered to be delayed subsources.

It should be noted that barriers which constitute limits of subsources can be divided into two different groups. Barriers of the first kind are more or less compatible with the model of plane crack: these are friction barriers, interlocks, surface waviness and so on. Barriers of another kind correspond to some stereometric obstacles; they can be compared with dislocation fission points of disclinations in elastic continuum theory. In particular, when a strike-slip rupture propagating along a fault strike meets a fault bend or kink either pure shear must change to partial tensile motion (and this needs much work to compensate rock pressure or to press out wedges of excess material) or secondary shear rupture would occur to compensate the change of direction of Burgers vector. Fault bifurcation can present no obstacle (but makes movement on two fault branches relatively independent). Step-like or en-echelon fault patterns may involve weak or strong obstacles depending on the relative orientation of steps to slip direction. A rather complicated secondary rupture system must accompany the main rupture when it passes along a fault twist (dip change). It is worth noting that when a dip-slip rupture propagates along a fault strike, bends and steps present no strong obstacles, only twists do. (In general, stereometric barriers need a non-planar rupture surface, but the opposite is not true: the generalized cylindrical rupture surface with its element along the slip vector presents no obstacles.) In conclusion we can say that there are plenty of modes to generate barriers and subsources in a real earthquake rupture process. We shall generally refer to them below as 'roughness'.

We noted above that there is another approach to the stochastic description of a source (Aki 1967; Haskell 1966; Andrews 1981). These papers introduce a space–time autocovariance function or corresponding power spectrum. This approach is more accurate formally, but it is not clear how it can be modified to describe in proper detail the observed characteristics of source radiation.

The main assumption of the proposed approach is incoherence or randomness of subsource 'switching on'. With this randomness, the main parameters of the subsource population are their space–time density and size–duration distribution. In a full model these parameters should be determined from dynamic considerations. Here we only postulate that such parameters do exist.

A relation between the reported concept and empirical data can be made clear if we note that the radiation spectrum of a real source is the superposition of radiation from the 'main smooth source' and incoherently combined radiation from the subsource population. For simplicity, let us suppose that all subsources are kinematically similar, then different kinds of source spectra can be interpreted as produced by subsource populations with different distribution functions. Such an idea can be accepted at least as a first approximation.

Let us consider first the space–time distribution of subsources. Results obtained by Kopnichev & Shpilker (1978) suggest that the usual mode of main rupture growth, which is manifested in the far field by roughly triangular or trapezoidal displacement pulses, is accompanied by the high-frequency radiation pulse of an analogous envelope shape. The most natural hypothesis is that the high-frequency incoherent radiation flux, together with the subsource density, is determined mainly by the local velocity of 'smooth' shear sliding. For the brittle crack model (and for the dislocation model) the zone of high sliding velocity occupies in any one moment only a relatively small part of the rupture area. It can be hypothesized, however, that in a real source this zone is rather wide. In any case, no such effects are taken into account in calculations carried out in this study. The rupture area is supposed to radiate with a power that is constant in space and time, so subsources are assumed to be distributed evenly. Some implications of violation of this assumption are discussed below.

Size and duration (or characteristic time) distribution of subsources is manifested

immediately in the source spectrum, but it is too early to carry out its profound analysis. It should be noted that both Shebalin (1971) and Blandford (1975) and then Hanks (1979) proposed the power-law size distribution of subsources. Equivalent assumptions of self-similitude of dislocation spectrum were made by Nur (1978) and Andrews (1980). It can be easily shown that a 'standard' f^{-2} displacement spectrum corresponds to $N(L) \propto L^{-2}$ size distribution, the same one as can be deduced from a frequency–magnitude distribution of independent earthquakes (Hanks 1979). But this simple assumption is not justified by shapes of observed spectra. Large ($M \approx 8$) earthquakes have a well-pronounced 'knee' in this displacement spectrum (Aki 1972; Zapolskii *et al.* 1973; Gusev 1979; Koyama, Takemura & Suzuki 1980). The corresponding frequency is about 0.1–0.3 Hz, thus demonstrating a sharp decrease in density of subsources with a size above 10–30 km.

Moreover, in its high-frequency part, the source spectrum is not self-similar. At frequencies above 5–15 Hz the observed near-field accelerogram spectra fall down appreciably. This observation can be compared with the lack of small earthquakes with a source size below some definite limit (Rautian *et al.* 1978; Chouet, Aki & Tsujiura 1978). This leads to the conclusion that another characteristic length exists (in the range of 100–500 m) which is the lower limit of subsource size. In such a complex situation we considered it undesirable to introduce any parametrical (power law or more complex) spectral shape model. We shall base our model instead directly on the average empirical spectra.

However, power-law subsource size distribution can be accepted as a zero approximation in order to obtain some information on subsource space distribution. As can be seen from Fig. 3, the spectral shape for earthquakes with $M = 5.5–7.7$ between corner frequency and second characteristic frequency (about 5 Hz) behaves as $f^{-(1.4-1.8)}$. Following Hanks (1979), we can derive that this trend corresponds to $N(L) \propto L^{-(3.2-2.4)}$. The L^{-3} law arises when subsources of some definite size range fill all the space–time volume of the source process (it is an obvious implication of the fact that for a single subsource this volume is proportional to L^3). L^{-2} law arises when subsources of some definite log size range occur only once at any point of source surface. This situation arises when running line (or crack tip) is switching subsources on. We have noted that we consider the real situation as more alike to the first case (with $f^{-1.5}$ trend).

The proposed way of describing the source radiation implicitly considers source function and radiation pulse as a quasi-stationary random process. This concept can be confirmed by the rather similar envelope shape of short-period P radiation pulses for different bands of the ChISS instrument (Zapolskii *et al.* 1973 and later publications by the same authors) for several large earthquakes. Quasi-stationariness is related to supposed overlapping of sources of different sizes. Some overlapping must exist; in an opposite case, when we suppose that for any frequency band there is an ensemble of isolated patches which produces it, we must imagine unrealistically high initial stress. For instance, let us consider a patch that generates $f \approx 5$ Hz in $M = 8.2$ source with 10 m slip, its initial deformation must be of the order of 10^{-2}, which is high above rock strength.

The energy spectrum description of a source, supposing its incoherence implicitly, was proposed by Riznichenko & Seiduzova (1972); some interesting approaches to simulation of incoherent source radiation were proposed by Rautian (1976) and Kopnichev & Shpilker (1978). Papers by Page, Boore & Dieterich (1975) and Rascon & Cornell (1969) should also be mentioned.

Hypothesis for short-period power flux stability and scaling relations

Assuming a radiator incoherence and a stability of radiation parameters within its area and duration, produces the most convenient description of a source in terms of spectral power

and spectral power flux. Following Riznichenko, let us introduce a logarithmic source energy spectrum

$$E(f) = \partial E / \partial \log f \tag{7}$$

and logarithmic spectral power flux

$$g(f) = \partial E / \partial S \, \partial t \, \partial \log f. \tag{8}$$

We now introduce full G and short-period G_{sp} energy flux

$$G = 2 \int_{-\infty}^{\infty} g(f) d \log f \tag{9}$$

$$G_{sp} = 2 \int_{-0.5}^{\infty} g(f) d \log f. \tag{10}$$

Our working hypothesis will be that $g(f)$ for short-period radiation and G_{sp} depend only weakly on the source size. In order to test this hypothesis, empirical data on $g(f)$ are needed. So we need $E(f)$, area S and characteristic time T. In order to simplify calculations, it would be convenient to use average scaling laws and similitude considerations. From the discussion above it must be clear that similitude can only be assumed for 'main smooth source'. To study this question in detail, let us consider a hypothesis for the 'strict' similarity, i.e. all characteristics of the main source are functions of only a single dimensional parameter. In theory, the most natural parameter to choose is the length L, but when considering observational data, the more convenient parameter is the seismic moment

$$M_0 = \int_{\Sigma} \mu B dS = \mu \bar{B} S$$

where $B = B(x,y)$ is the cumulative dislocation (slip) in a point (x,y) on the fault, and Σ is the source surface, assumed to be flat. Strictly speaking, slip is a vector, but here we assume that the direction of slip is the same everywhere within the source. For 'strict' similitude it is obvious that

$$\bar{B} \propto L \propto T \propto M_0^{1/3} \propto S^{1/2}. \tag{11}$$

Only seismic energy of the main source is scaled

$$E_{main} \propto M_0 \propto L^3.$$

Many sets of source parameters have recently been published and several authors have demonstrated that the hypothesis for similitude is reasonable. We compiled from published data the average world correlations of L, T, $\bar{B}$ and E with M_0 (Fig. 1). In most cases initial data were plotted as a function of magnitude. To convert such correlations into M_0 scale, average relations between M_{LH}, M_s and M_L and M_0 were also compiled and then used for conversion. In constructing the curves in Fig. 1, much attention was paid to the independence of curves. Namely, $L(M_0)$ curve was compiled mainly from field measurements, aftershock and tsunami data, $\bar{B}(M_0)$ from field data only, $T(M_0)$ from spectral data. The $E(M_0)$ curve is of relatively low reliability. The range of the main part of data is shown on the curves. A detailed description of the compilation of Fig. 1 with references will be published separately.

Examination of Fig. 1 shows that a 'strict' similarity hypothesis seems reasonable on the average for earthquakes of $M = 5–8$ and is violated for smaller events. Yet the range of individual data is great, greater than 0.5 order of magnitude. The three most important

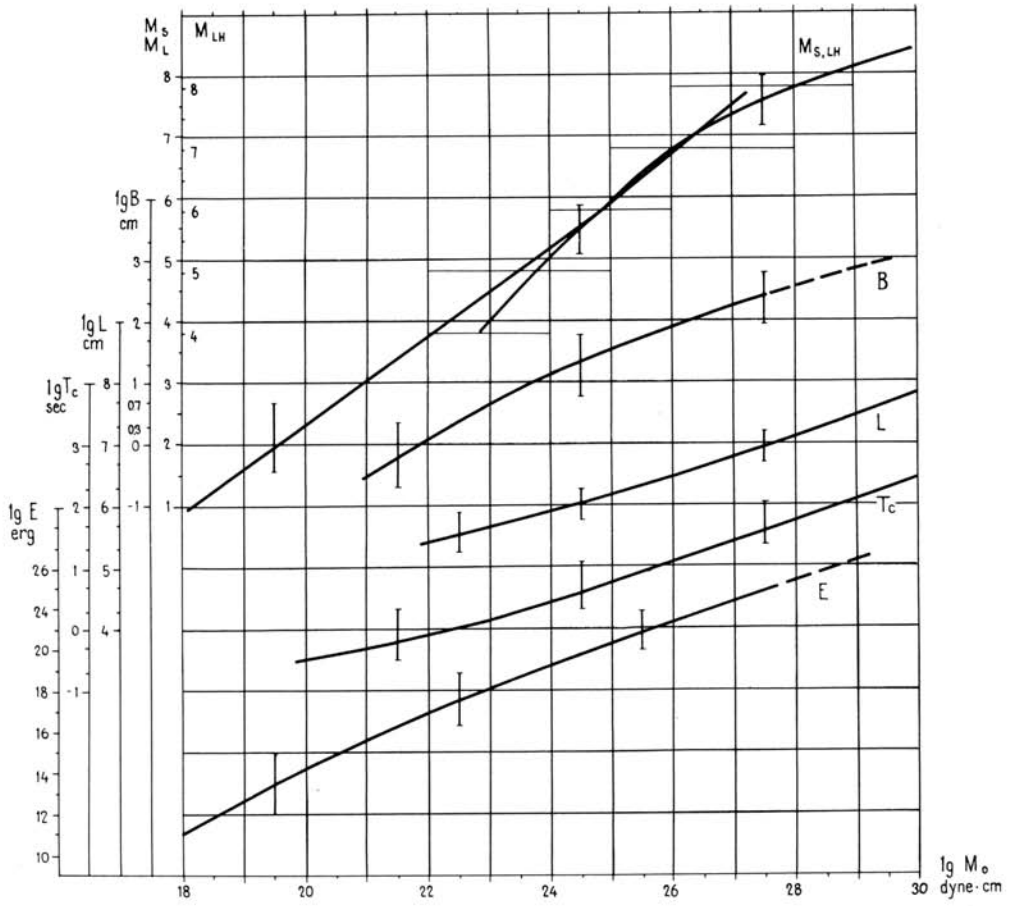

Figure 1. Average relations between seismic moment M_0 and earthquake parameters: magnitudes M_{LH}, M_S and M_L (upper left curve), average dislocation $\bar{B}$, source length L, characteristic time T and seismic energy E.

dimensionless parameters which must be stable in order for the 'strict' similarity hypothesis to hold true are: (1) relative width $w = W/L$ (the ratio of the source width W to its length L); (2) strain drop $\Delta\epsilon = (1/\mu)\,\Delta\sigma \approx \bar{B}/W$ and (3) Mach number $\nu = v/c_S$; v being the rupture propagation velocity and c_S the shear wave velocity. The stability of w was studied by Vostrikov (1973) and Geller (1976), who have both found w to be stable on average, with typical value $w = 0.5$. The stability of $\Delta\sigma$ was studied by Thatcher & Hanks (1973) and Kanamori & Anderson (1975). $\Delta\sigma$ was found to be relatively stable in the magnitude range 5–8, with typical values 30–50 bar, so $\Delta\epsilon$ is near to 1×10^{-4}. No data exist to assume a large instability of ν; a typical value 0.6 was accepted for further calculations. Thus the 'strict' similarity hypothesis can be accepted as an average for large earthquakes. A slight maximum of $\Delta\sigma$ should be mentioned in the range $\log M_0 \approx 26$ ($M \approx 6.5$), this agrees with results obtained by Chouet *et al.* (1978).

Construction of the set of average spectra

We shall use the term 'source spectrum' (Aki & Chouet 1975; Rautian *et al.* 1978) to designate the module of Fourier transform $\dot{M}_0(f)$ of moment rate of equivalent point force dipole. As is well known, $\dot{M}_0(0) = M_0$. We assume that the source spectrum is averaged by

the point source directivity function and by directivity related to the time history of a finite source.

The main subject of our discussion will be the source spectrum average for different earthquakes with the same M_0. We suppose it useful to consider such a concept in spite of unavoidable dispersion of individual spectra. Nevertheless, M_0 is the most important scaling parameter, and we shall search for the average relationship between $\dot{M}_0(f)$ and M_0.

To compile such a relationship, diverse data sources were used, but the basic data set was the system of average accelerogram spectra for the western USA compiled by Trifunac (1976b). Average spectra for the horizontal component at $r = 25$ km on the rock ground for $M_L = 4.5$, 5.5, 6.5 and 7.5 were first corrected for attenuation. A frequency-dependent Q was accepted

$$Q_S = \begin{cases} Q_0 & f \leqslant 1 \text{ Hz} \\ Q_0 f^{\gamma} & f > 1 \text{ Hz} \end{cases}. \tag{13}$$

with $Q_0 = 250$ and $\gamma = 0.5$. Then the correction was made for the source finiteness effect by a technique which will be clear from calculations given below. This correction is minor, however, being only +0.15 log units for $M = 7.5$, when it attains its maximum.

Some unessential factors aside, the set of spectra obtained corresponds to $f^2\dot{M}_0(f)$ curves in the frequency band 0.3–20 Hz. In order to extrapolate spectra to lower frequencies, the low frequency branches of $f^2\dot{M}_0(f)$ function were calculated according to the formula

$$f^2\dot{M}_0(f) = \frac{f^2 M_0}{1 + (f/f_0)^{1.7}}, \tag{14}$$

where $f_0 = f_0(M_0) = T^{-1}(M_0)$ from Fig. 1, and M_0 values correspond to M_L values mentioned above according to the $M_L(M_0)$ curve on the same plot. High- and low-frequency branches were adjusted to one another in the frequency range 0.2–0.5 Hz. Spectra obtained were then replotted on the plane $\dot{M}_0$, M_0 with f as a parameter (Fig. 2). In the same graph the relationship $\dot{M}_0(M_0)$ for 0.3 Hz was plotted – this was derived from average spectra for Japanese earthquakes (Koyama *et al.* 1980). The agreement proved to be good. The agreement is worse for Tadgikistan data from Rautian *et al.* (1980). The curve $M_s(M_0)$ from Fig. 1 was considered as the relationship $\dot{M}_0(0.055, M_0)$ and was also plotted.

Of specific interest was a construction of the $\dot{M}_0(M_0)$ curve for the frequency band around 1 Hz. For this we have used some indirect but reliable techniques. We combined: (1) the 1-Hz frequency band (ChISS) magnitude m_1 versus m_{PV}^{SK} relation (Zhbrykunova & Zhbrykunov 1974); (2) the m_{PV}^{SKM} versus m_{PV}^{SK} relation from Fedorova *et al.* (1974) and Khalturin (1974); (3) the m_{PV}^{SK} versus M_{LH} relation from Kondorskaya, Gorbunova & Landyreva (1974) and (4) the M_{LH} versus M_0 relation according to Fig. 1. Values of m_1 were converted to log spectral density, according to equations (37) and (38) listed below and Parceval's theorem. It was found that in the magnitude range 4–6, the P-wave spectrum increases somewhat steeper than the S-wave spectrum, but for large magnitudes trends of both spectra (P from m_1 and S from acclerograms) practically coincide. The most promising feature of the three curves for 1.0, 0.32 and 0.055 Hz is their almost identical trend in the magnitude range 6–8; this allows us to extrapolate $\dot{M}_0(f)$ reliably to larger M_0 values in the frequency range 0.05–1 Hz.

For higher frequencies, trends of $\dot{M}_0(M_0)$ seem to be slower than $\dot{M}_0(1 \text{ Hz}, M_0)$, and this difference may be real. But we could not obtain any reliable estimates of this trend; and we preferred to extrapolate $\dot{M}_0(M_0)$ for higher frequencies by analogy with $M_0(1 \text{ Hz}, M_0)$. This may have led to some overestimation in our results.

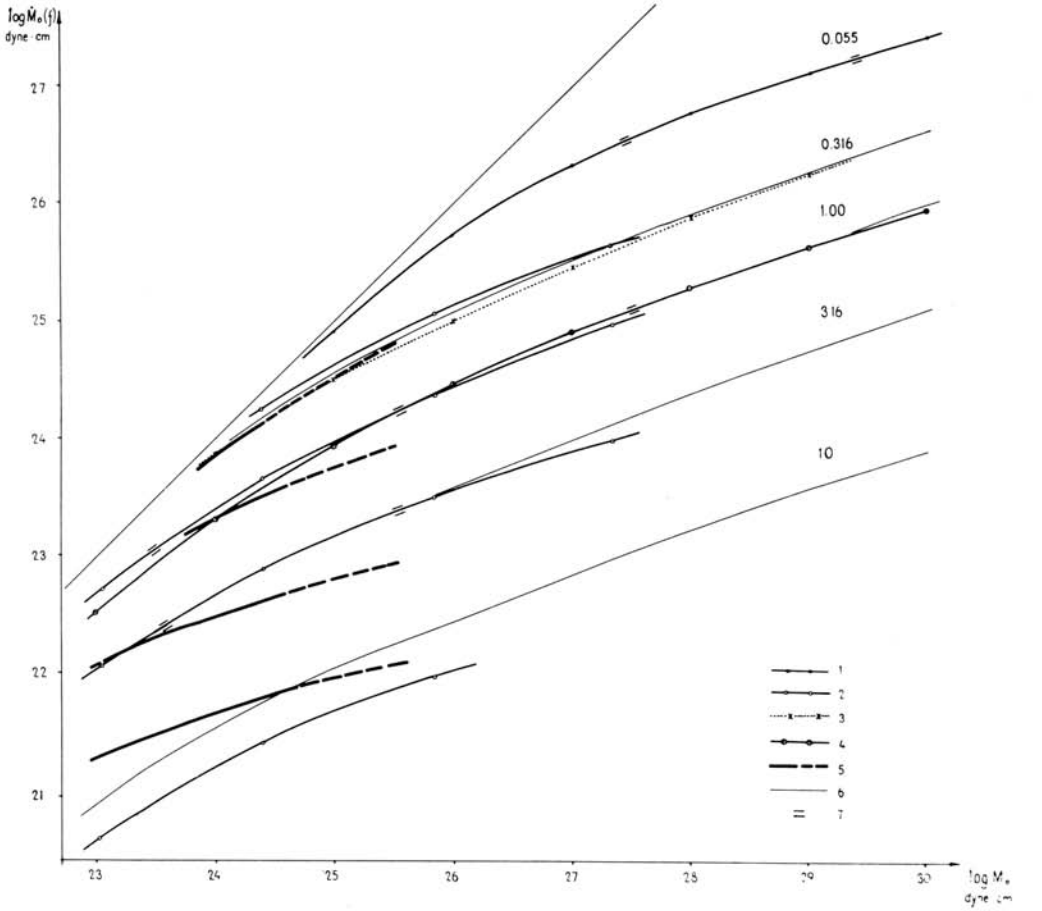

Figure 2. $\dot{M}_0(f)$ versus M_0 relation for fixed frequencies f = 0.055, 0.1, 0.32, 1.0, 3.2 and 10 Hz. (1) M_{LH} curve from Fig. 1 as $\dot{M}_0(0.055)$. (2) Curves derived from accelerogram spectra of the western USA. (3) Curve for 0.32 Hz derived from fig. 6 in Koyama *et al.* (1980). (4) Curve for 1 Hz derived from magnitude relations (see text), its level is determined by coincidence with curve 2 at $M = 6.5$. (5) Curves for Tadgikistan, according to fig. 14 in Rautian, Khalturin & Zakirov (1980). (6) Extrapolated parts of curves. (7) Parts of initial curves used without change.

A marked difference is observed for the same frequency range between Californian and Tadgikistanian spectra. This difference seems to demonstrate regional variations of spectral shape, determined by the number and characteristic size of heterogeneities in the faults. After examining a number of accelerogram spectra from different parts of the world and considering the evidence of the upper limit of small earthquake corner frequencies we could conclude that the regional differences are very pronounced in this spectral range. In such a situation no clearly defined 'world average' can be considered, and some compromise is needed. For further calculations we have accepted, somewhat arbitrarily, the 'Californian' shape but with less pronounced decrease at frequencies of above 3 Hz (according to the $f^{-2.5}$ law for a displacement spectrum). By extrapolating the corresponding spectral levels to large M_0 values parallel to the $\dot{M}_0$ (1 Hz, M_0) curve, we finally obtained $\dot{M}_0(f)$ values for large earthquakes. For the frequency range 0.01–0.05 Hz spectra of large earthquakes were

estimated again by adjusting a theoretical model

$$\dot{M}_0(f) = \frac{M_0}{1 + (f/f_0)^\gamma}$$

(where γ was taken to be 2.2 for the best fit) to the constructed part of spectral set. It was the last step in the construction of the whole spectral set. Values of $f^2 \dot{M}_0(f)$ are plotted in Fig. 3, they determine the shape of acceleration spectra in the far field (neglecting absorption).

The main differences of the constructed set of curves from any set derived by assuming similitude are:

(1) There are two characteristic frequencies: $f_1 \approx 0.2$ Hz and $f_2 \approx 5$–15 Hz, independent of M_0, which are distinctly expressed in the spectral shape. (2) When M_0 increases, the growth of the short-period spectral level becomes slower for $\log M_0$ when above 26–27 ($M \approx 7$–7.5). This is evidence of relatively low short-period radiation capability of the surface of large sources.

Test of hypothesis for power flux stability

According to our construction technique, spectra in Fig. 3 correspond to observations on the Earth's surface. Source spectra as such should be corrected for impedance differences

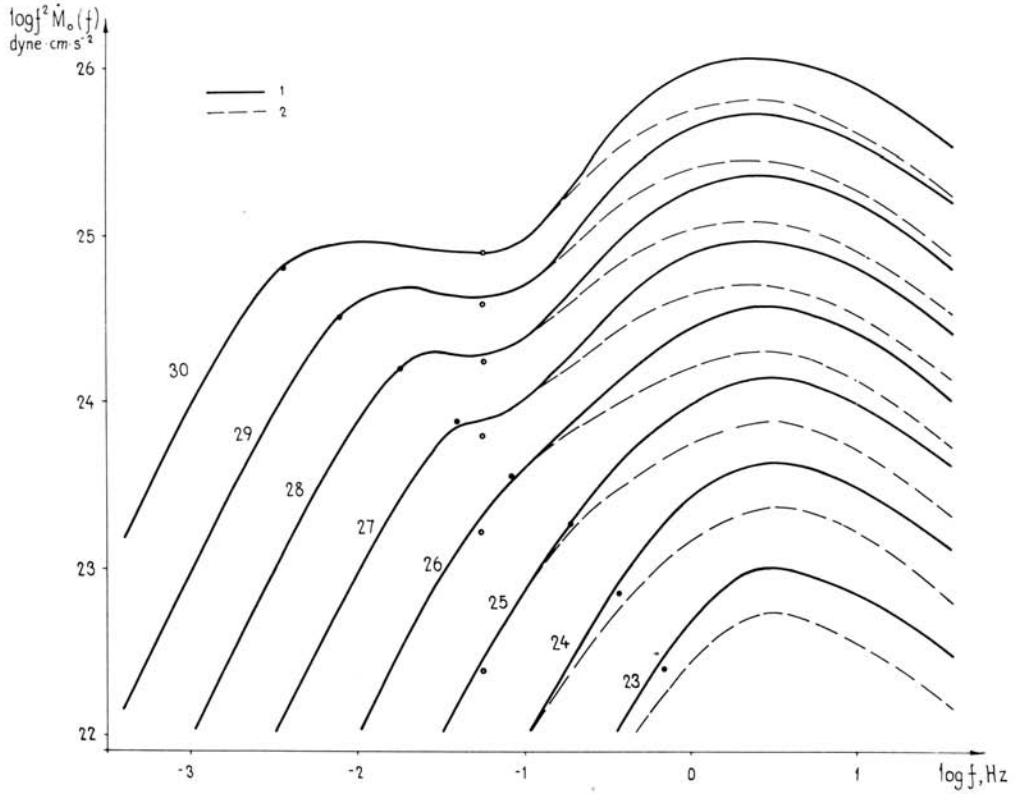

Figure 3. A set of average spectra of value $f^2 \dot{M}_0(f) = (2\pi)^{-2} \ddot{M}_0(f)$ for $\log M_0 = 23$–30. Continuous lines: spectra as observed at the Earth's surface, broken line: reduced to the source. Points: spectral level at corner frequency according to the model $\dot{M}_0(f) = M_0 [1 + (f/f_0)^\gamma]^{-1}$. Circles: spectral level derived from $M_{LH}(M_0)$ curve.

between the source vicinity and the Earth's surface. As a first approximation, this correction may be estimated for a layered medium with a smooth velocity profile. For a hypothetic average profile, the following set of corrections was obtained:

f, Hz	0.1	0.32	1	3.2	10
$\delta \log \dot{M}_0(f)$	0.0	−0.12	−0.25	−0.30	−0.30

Spectra $\dot{M}_{00}(f)$ corrected in this way were used to test our initial hypothesis for the relative stability of the average short-period power flux G_{sp} from the surface of a source of any size. For this purpose integrals were computed

$$I(M_0) = \int_{-0.5}^{1} f^3 \dot{M}_{00}^2(f)\, d \log f. \tag{15}$$

To estimate G and G_{sp}, a somewhat modified expression from Dahlen (1974) for S-wave energy was applied:

$$E(f) = \frac{k_R \ln 10}{16 \pi^2 \rho c_S^5} \dot{M}_0^2(f) f^3 \tag{16}$$

where

$$k_R = \frac{1}{4\pi} \int_0^{\pi} d\theta \int_0^{2\pi} \mathbf{R}_S(\theta, \rho)\, d\rho \tag{17}$$

is the average square of directivity function $\mathbf{R}_S$ for full vector displacement in the S-wave. Dividing $E(f)$ by source area $S \approx \pi LW/4$ and process duration T, we obtain the estimate for $g(f)$ as

$$g(f) = E(f)/S \cdot T. \tag{18}$$

Using the dimensionless parameters introduced above, and integrating by $\log f$, we obtain

$$G_{sp} = \frac{8 \ln 10 w \nu\, \Delta\epsilon}{5 c_S^2} [2I(M_0)/M_0]. \tag{19}$$

Numerical values for w, ν and $\Delta\epsilon$ are listed above, $c_S = 4$ km s^{-1} and $I(M_0)$ values obtained by numerical integration were substituted to obtain values of G_{sp} in the narrow range $1-6 \times 10^7$ erg cm^{-2} s for different M_0 values. A maximum is reached at $\log M_0 = 25-26$, and minimum values are found at the ends of the M_0 range examined ($\log M_0 = 23-30$). The total power flux was estimated in the same way, giving values $2-8 \times 10^7$ erg cm^{-2} s. Finally, seismic efficiency (radiated to elastic energy ratio) was estimated assuming a 100 per cent stress drop ($E_{elastic} = \frac{1}{2} \Delta\epsilon M_0$); it is 10–25 per cent.

Low values of G_{sp} for small and very large earthquakes have different origins. The cause is low $\Delta\epsilon$ and a narrow spectral band for small earthquakes, while the low radiation capability mentioned above accounts for very large ones. The last phenomenon is very important. We suppose its physical cause is as follows: an $M \approx 8$ earthquake source is wider than the width of the effectively brittle layer of the lithosphere, and a large part of its surface is unusually smooth and depleted in asperities and interlocks. This leads to two implications. First, at low frequencies ($f \approx 0.1$ Hz) the inclined higher-frequency branch of the displacement spectrum behaves as $f^{-2.2}$ instead of $f^{-1.7}$ for smaller events, producing a 'knee' in the source spectrum. Secondly, when M_0 and W increase, the 'normal' short-period radiation is generated by a continuously lessening part of the source area, thus decreasing the average G_{sp}. If this explanation is accurate, the upper limit of the subsource width should

coincide with a width of the 'normal' part of the source area. The last value is near to the normal width of a seismically active zone, which is usually 10–30 km. Taking 15 km as a typical value, we get a subsource with corner-frequency $f_0 = (L/vc_S)^{-1} = 0.14$ Hz and $M_0 = 25.3$. The first value coincides with the characteristic frequency f_1 of our spectra, the second is only somewhat lower than the typical value of $\log M_0$ for the largest subsources, according to Stewart & Kanamori (1978). Thus our initial explanation looks reasonable. The vertical inhomogeneity of the generation of short-period 'macroseismic' radiation was observed by Shebalin (1974), who also found that the upper part of the large source surface radiates more intensely.

It should be clearly noted that we only deal here with average trends. Large individual variations in short-period radiation capability do exist, the most prominent of them being correlated with a focal mechanism (Kopnichev & Shpilker 1978; Gusev 1979; Kopnichev, Nersesov & Medvedeva 1980; Aptikaev & Kopnichev 1979), but regional variations are also present. We believe that the difference in fault surface roughness plays the key role in these variations. Roughness characteristics define parameters of a certain non-linear transformation, which converts low wavenumber energy of smooth sliding in the main source to high wavenumber and high-frequency energy of incoherent radiation (*cf.* Andrews 1980). This transformation is local by nature, so no simple and direct correlation between $\Delta\sigma$ (which is the global, essentially dimensionless, characteristic of low wavenumber elastic energy) and G_{sp} should exist.

Derivation of estimates of short-period amplitudes in the near field

Results obtained above are based on an equivalent point representation of the source. In order to test our concept against the near-field data, some theory for short-period radiation from a finite incoherent source should be developed. Housner (1955) was the first to suggest a model of this kind.

In the vicinity of a source the elastic field consists of wave and static terms (Haskell 1964) (more accurately now there are two wave terms, two static terms and a 'transient static term'). Let us first estimate a contribution from a static term. From considerations of continuity, 'static' acceleration in the immediate vicinity of the fault is near to

$$a_{st} \approx 0.5\,\ddot{B}, \tag{20}$$

where $\ddot{B} = \partial^2 B/\partial t^2$; $B = B(t)$ – local dislocation. At first glance, $\ddot{B}$ can be estimated as follows:

$$\overline{\ddot{B}^2(f)} \approx \left(\frac{2\pi f \dot{M}_0(f)}{\mu S}\right)^2 \tag{21}$$

(the line above denotes averaging). This expression is valid, however, only for coherent radiation. For short-period incoherent radiation the contributions from different sufficiently small spots of the source are added energetically; the observed $\dot{M}_0(f)$ being the result of such summation and hence should be corrected. We assume now that the correlation radius of the source function is the least possible, equal to half of the wavelength $\lambda = c_S/f$ for radiation in a frequency band around f, so

$$R_{coh} = c_S/2f. \tag{22}$$

In this case the source consists of $N \approx S/\pi R_{\mathrm{coh}}^2$ statistically independent radiatiors, and the correction factor we look for is $N^{0.5}$ for amplitude or N for square amplitude. Thus

$$a_{\mathrm{st}}^2(f) = \frac{1}{\pi S}\left(\frac{2\pi f^2 \dot{M}_0(f)}{\mu c_S}\right)^2. \tag{23}$$

Therefore, though the static field and the wavefield are proportional to B and $\dot{B}$ respectively, because of incoherence, the far-field wave spectrum and near-field static spectrum are of the same shape. This result is only an estimation; for power-law spectra it was derived more accurately by Andrews (1981).

To obtain numerical values, we shall model the time history of a_{st} by a segment of a Gaussian process with equivalent duration $\tau_{\mathrm{eq}} = 0.4T$; then

$$\tfrac{1}{2} a_{\mathrm{ste}}^2 \tau_{\mathrm{eq}} = \overline{2a_{\mathrm{st}}^2(f)}\,\Delta f \approx 2a_{\mathrm{st}}^2(\bar{f})\,\Delta f, \tag{24}$$

where a_{ste}^2 is the mean square extremum of time-function, $\bar{f}$ is the average weighted frequency (near to peak frequency) and Δf is the effective bandwidth. In consequence

$$a_{\mathrm{ste}} = \left(\frac{8\pi \Delta f}{0.4TS}\right)^{1/2} \frac{f^2 \dot{M}(f)}{\mu c_S}. \tag{25}$$

For $\log M_0 = 26$ we accept (see Figs 1 and 3) $\bar{f} = 4.8$ Hz, $\Delta f = 8.2$ Hz, $\log [f^2 \dot{M}_{00}^2(\bar{f})] = 24.42$, $T = 11.7$ s, $S = \pi LW/4 = 312$ km^2. Let $c_S = 4$ km s^{-1}, $\mu = 5 \times 10^{11}$ dyne cm^{-2}, then

$a_{\mathrm{ste}} = 69$ gal.

This estimate is minimal. According to results obtained by Geller (1976), movement in any point takes, on average, only 1/5 of the duration of the whole process. So our estimate increases $\sqrt{5} = 2.3$ times, that corresponds to $a_{\mathrm{ste}} = 155$ gal. The a_{ste} value will rapidly decrease with distance from the fault surface, as a result of both incoherence ('phasing out') and r^{-2} geometrical attenuation; so the static term for $f = 1$ Hz and greater can be assumed to be negligible at distances of more than 1–2 km from the fault.

Let us now estimate the wavefield (we shall limit ourselves to S-waves and neglect the P-wavefield). A somewhat analogous approach was suggested by Rautian (1976) at a conceptual level. We assume that the elementary source is isotropic and its wavefield is isotropically polarized. Then the displacement in the wavefield of the elementary radiator dS is

$$du(\xi, \eta, \zeta, t) = \frac{k_{\mathrm{R}}^{1/2} \mu \dot{B}(x, y, t - r/c_S)\, dS}{4\pi \rho c_S^3 r} \tag{26}$$

and the square displacement from the whole source is

$$u^2(\xi, \eta, \zeta, t) = \frac{k_{\mathrm{R}} \mu^2}{16\pi^2 \rho^2 c_S^6} \int_{\Sigma} \int_{\Sigma'} \frac{\dot{B}(x, y, t - r/c_S)\, \dot{B}(x', y', t - r'/c_S)\, dS\, dS'}{rr'}, \tag{27}$$

where Σ and Σ' are two copies of the source surface with coordinates (x, y) and (x', y') on them; ξ, η and ζ are the coordinates of an observation point; $\zeta = 0$ is the plane of the source surface; $r = [(x - \xi)^2 + (y - \eta)^2 + \zeta^2]^{1/2}$, $r' = [(x' - \xi)^2 + (y' - \eta)^2 + \zeta^2]^{1/2}$. Factor $k_{\mathrm{R}} = 0.4$ is the same as in (17). Denote the double integral as I, rewrite it as a double sum and take the ensemble mean (line above), assuming $\dot{B}$ to be normally distributed:

$$I = \int_{\Sigma}\int_{\Sigma'} \frac{\overline{\dot{B}(x,y,t-r/c_S)\,\dot{B}(x',y',t-r'/c_S)}\,dS\,dS'}{rr'} \approx \sum_i \sum_j \frac{\overline{\dot{B}_i(t-r_i/c_S)\dot{B}_j(t-r_j/c_S)}\,\Delta S_i\,\Delta S_j}{r_i r_j}$$

$$= \sum_i \sum_j \frac{\left[\overline{\dot{B}_i^2(t-r_i/c_S)}\right]^{1/2}\left[\overline{\dot{B}_j^2(t-r_j/c_S)}\right]^{1/2}\rho_{ij}\,\Delta S_i\,\Delta S_j}{r_i r_j}. \tag{28}$$

Here ρ_{ij} is the correlation coefficient of $\dot{B}$ between two small areas ΔS_i and ΔS_j, and incoherence implies that ρ_{ij} can be assumed to be δ_{ij} (Kroeneker delta). Let all ΔS_i be of equal area, S/N, and let us introduce the average value $\dot{B}_0^2$ of $\dot{B}_i^2$ in different spots, then we can rewrite (28) as

$$I = \frac{\dot{B}_0^2 S}{N} \sum_i \frac{\Delta S_i}{r_i^2} \approx \frac{\dot{B}_0^2 S}{N} \int \frac{dS}{r^2} = \frac{\dot{B}_0^2 S}{N} \cdot I_1. \tag{29}$$

In the far field $I_1 = S/r^2$ and

$$u^2 = \frac{k_R \mu^2}{1b\pi^2 c_S^6 \rho^2} \cdot \frac{\dot{B}_0^2 S^2}{Nr^2}. \tag{30}$$

From another side, from (26), again introducing $\dot{M}_0(t)$ for an equivalent point source, we obtain

$$u^2(t) = \frac{k_R \dot{M}_0^2(t)}{16\pi^2 c_S^6 \rho^2 r^2}. \tag{31}$$

Comparing (30) and (31), the unknown combination $\dot{B}_0^2 S/N$ can be eliminated from (29) and finally we have

$$\overline{u^2(\xi,\eta,\xi,t)} = \frac{k_R \dot{M}_0^2(t) I_1}{16\pi^2 c_S^6 \rho^2 S}. \tag{32}$$

We calculated I_1 for the simplest case, when the observation point is on the axis of a disc source of radius R, at a distance h from its centre, then the resulting expression is

$$I_1 = \pi \ln (u^2 + h^2)\Big|_{u=0}^{u=R}. \tag{33}$$

When $h = 0$ (observation point on Σ), the integral diverges at the lower bound; this is related to 'absolute incoherence' ($\Delta S \to 0$). So the lower bound ehanges to R_{coh}. In further calculations we assume $R_{\text{coh}} = c_S/2\bar{f}$, where $\bar{f}$ is the mean frequency of the spectrum. We thus obtain

$$\overline{u^2(0,0,h,t)} = \frac{k_R \dot{M}_0^2(t)}{16\pi^2 \rho^2 c_S^6}\left(\frac{1}{R^2} \ln \frac{R^2 + h^2}{R_{\text{coh}}^2 + h^2}\right). \tag{34}$$

For $h \gg R$, the factor in brackets is asymptotically equal to $1/h^2$ and corresponds to $1/r^2$ in the initial expressions. Expression (34) will be applied as an approximation to the whole vicinity of the source surface. It is assumed to be elliptical, so R is substituted by $R_{\text{eff}} = {}^1\!/_2 (LW)^{1/2} \approx 0.4 L(M_0)$, and h by distance r_c from the source centre. Now let us use Parceval's

theorem and substitute $a(t) \equiv \ddot{u}(t)$ instead of $u(t)$:

$$\int_0^\infty a^2(t)\,dt = \int_{-\infty}^{\infty} (2\pi f)^4 u^2(f)\,df. \tag{35}$$

Introducing the effective duration τ_{eff}, the effective frequency bandwidth Δf and spectral peak frequency $\hat{f}$, we obtain root mean square acceleration:

$$a_{\text{rms}} = \left(\frac{2\Delta f}{\tau_{\text{eff}}}\right)^{1/2} \frac{k_{\text{R}}^{1/2} \dot{M}_0(\hat{f})\,(2\pi\hat{f})^2}{4\pi\rho c_S^3} \left(\frac{1}{R_{\text{eff}}^2} \ln \frac{R_{\text{eff}}^2 + r_c^2}{R_{\text{coh}}^2(\bar{f}) + r_c^2}\right)^{1/2}. \tag{36}$$

Here τ_{eff} and Δf are defined as the duration and bandwidth of a pulse or a spectrum with a boxcar envelope of equal energy and maximum value.

To obtain estimates which could be compared with observations in the near field, several corrections should be included. To take into account the effect of the free surface of the Earth, let us introduce factor $k_1 = 2$. Projection of the field vector into an arbitrary direction gives factor $k_2 = 2^{-0.5}$. The maximum from two components is generally referred to in empirical data lists; the corresponding correction is $k_3 = 1.5^{0.5}$. Ratio k_4 of the maximum extremum a_{max} to rms extremum a_{rmse} can be derived from the extremal value theory (Gumbel 1965), if the time history is assumed to be a segment of the Gaussian process.

$$k_4^2 = \ln n + 0.577 \tag{37}$$

where $n \approx 2\bar{f}\tau_{\text{eff}}$ is the number of extrema in the maximum part of time history. Ratio of a_{rmse} to a_{rms} gives the factor $k_5 = 2^{0.5}$.

In order to estimate the effective duration τ_{eff}, we shall assume that it is about 0.4 of the duration measures used in seismology. They usually correspond to a duration at the level of 20–30 per cent for amplitude or 5–10 per cent for power. Values of T in Fig. 1 are of this kind. But the value $\tau_{\text{eff}} = 0.4\,T$ is applicable only in the vicinity of a fault. With increasing distance, the time history lengthens because of wave scatter, dispersion in the surface waveguide and multi-ray wave propagation. As a first approximation, we shall assume that this effect can be represented by convolution of the envelope of the square of the source pulse with the square of the envelope of the pulse response of the medium. The last function is assumed to be frequency-independent (for simplicity only). Then, if the rms durations of these two functions are $\tau_{0\text{eff}}$ and $\tau_{\text{sc}}(r_c)$, the rms duration of their convolution is $[\tau_{0\text{eff}}^2 + \tau_{\text{sc}}^2(r_c)]^{1/2}$. According to Trifunac & Brady (1975), we can assume $\tau_{\text{sc}}(r_c) = k_\tau r_c$. The expression used was of the form

$$\tau_{\text{eff}} = 0.4\,[T^2 + (0.2 r_c)^2]^{1/2}, \tag{38}$$

where the factor 0.2 was estimated from experimental plots (Rautian & Nikiforova 1980); Trifunac's own estimate is about 0.15.

To account for attenuation, $f^2\dot{M}_0(f)$ values were corrected for frequency-dependent attenuation for distance r_c, with $Q(f)$ according to (13). The correction factor is $k_Q(f) = \exp[-\pi f r_c/Q(f)c_S]$. The frequency of the peak in $A(f) = k_Q(f) f^2 \dot{M}_0(f)$ is $\hat{f}$; the effective bandwidth Δf is determined as $(f_r - f_l)$, where f_l and f_r are left and right cut-off frequencies of $A(f)$ at the 0.5 level for power (0.7 for amplitude), and the mean frequency $\bar{f}$ is estimated as $(f_r + f_l)/2$.

We can now write the final formulae to be used for numerical calculations of rms acceleration:

$$a_{\mathrm{rms}}(M_0, r_c) = \frac{(2\pi)^2 k_R^{1/2} k_1 k_2 k_3 (2\Delta f)^{1/2} A(\hat{f})}{4\pi\rho c_S^3 \tau_{\mathrm{eff}}^{1/2}} \left(\frac{1}{R_{\mathrm{eff}}^2} \ln \frac{R_{\mathrm{eff}}^2 + r_c^2}{R_{\mathrm{coh}}^2(\bar{f}) + r_c^2} \right)^{1/2} \tag{39}$$

and of maximum acceleration:

$$a_{\max}(M_0, r_c) = k_4 k_5 a_{\mathrm{rms}} = \{2[\ln(2\hat{f}\tau_{\mathrm{eff}}) + 0.577]\}^{1/2} a_{\mathrm{rms}}. \tag{40}$$

Calculated and observed parameters for the near field

We shall start with estimates for the immediate vicinity of a fault. Taking $\log M_0 = 27$ ($M = 7.35$) and $r_c = 0$ (we shall delete the subscript c from now on), we obtain the following estimates for the 'average' earthquake

$a_{\mathrm{rmse}} = 600$ gal,

$a_{\max} = 1380$ gal,

$\bar{f} = 4.5$ Hz,

$f_1 = 0.8$ Hz,

$f_r = 8.4$ Hz.

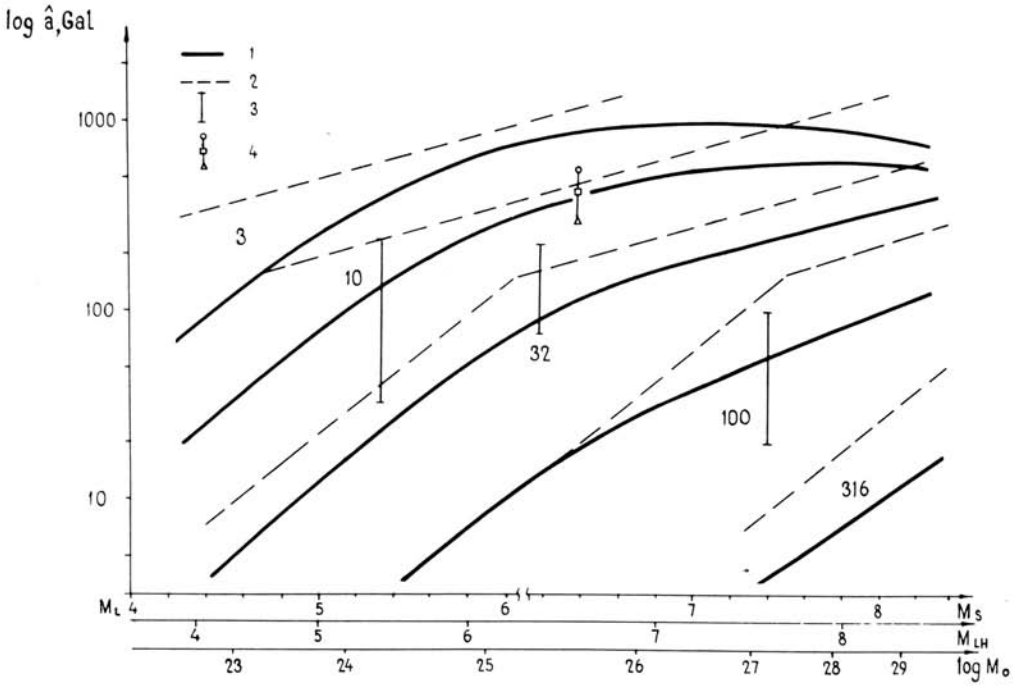

Figure 4. Calculated relation between maximum acceleration on firm ground $a_{\max}$ and magnitude for distances 3, 10, 32, 100 and 320 km from the source centre, as compared with empirical data. (1) Calculated curves. (2) World data set averaged by Aptikaev & Kopnichev (1979). (3) One-sigma boundaries for the western USA and Alaska according to Boore *et al.* (1980). (4) Estimates for $M = 6.4$, $r = 10$ km from three sources (see text).

Though these figures are interesting, it is difficult to compare them with observations. Calculations for some distances are more useful. We computed values of a_{max} according to the expression listed above; the results are shown in Fig. 4. A set of curves corresponds to $r = 3$, 10, 31, 100 and 316 km. Our results should be compared with observations of horizontal acceleration on firm ground. Fig. 4 compares the empirical correlations from Aptikaev & Kopnichev (1979), a range of estimates from Boore *et al.* (1980) and, for $r = 10$ km and $M = 6.4$, three estimates from Donovan (1973), Shnabel & Seed (1973) and Trifunac (1976a), reproduced from Boore *et al.* (1980). We consider the agreement to be satisfactory.

It should be noted that a small decrease of $a_{max}(M_0)$ in the vicinity of a source of a very large earthquake can be artificial, as we 'smeared' the total power uniformly over the source surface, whereas its upper part, nearest to the Earth's surface, radiates stronger. On the other hand, we could overestimate the spectral level when we accepted the same growth rate of $\dot{M}_0(M_0)$ for $f = 1-20$ Hz, and these uncertainties may compensate each other.

Also, it was of great interest to obtain a 'theoretical' relation of intensity I with M and r. In this calculation we used the formula

$$I = 3.3 \log a_{max} + 1.0 \log \tau_{eff} + \text{constant}. \tag{41}$$

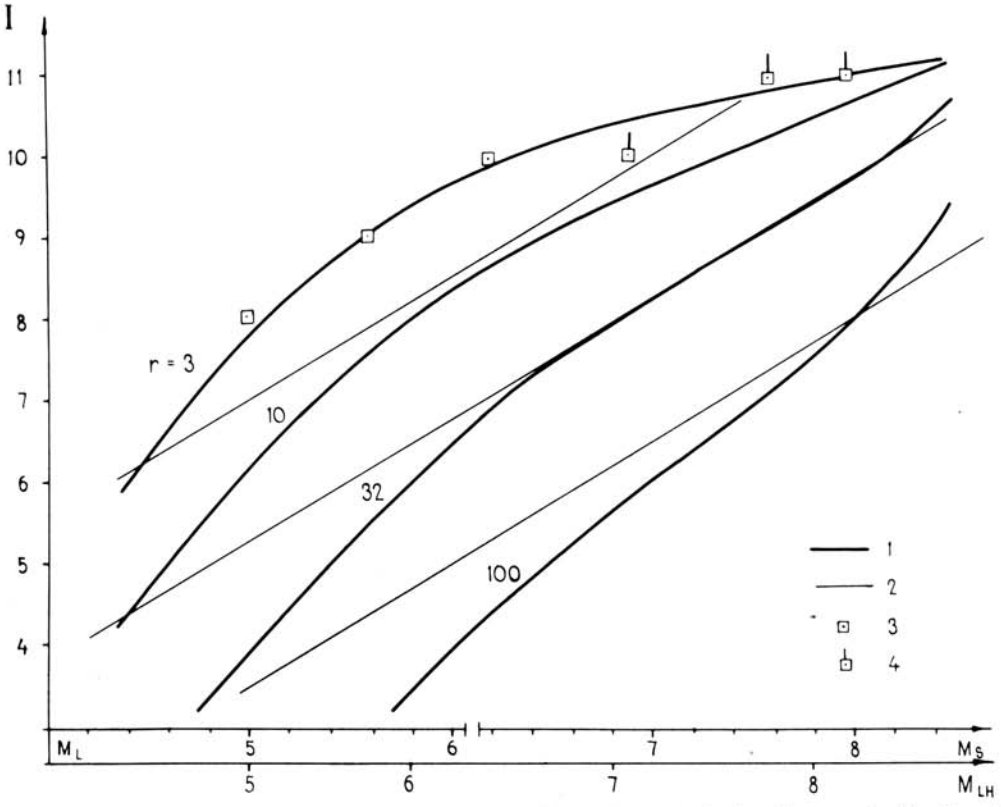

Figure 5. Calculated relation between intensity I (MSK) and magnitude for distances 3, 10, 32 and 100 km from the source centre. The level of calculated curves is selected for the best fit with the empirical relation. (1) Calculated curves. (2) Empirical relation according to Shebalin (1976). (3) and (4) Upper limits of intensity and lower bound of upper limit of intensity in epicentral zone according to Shebalin (1974).

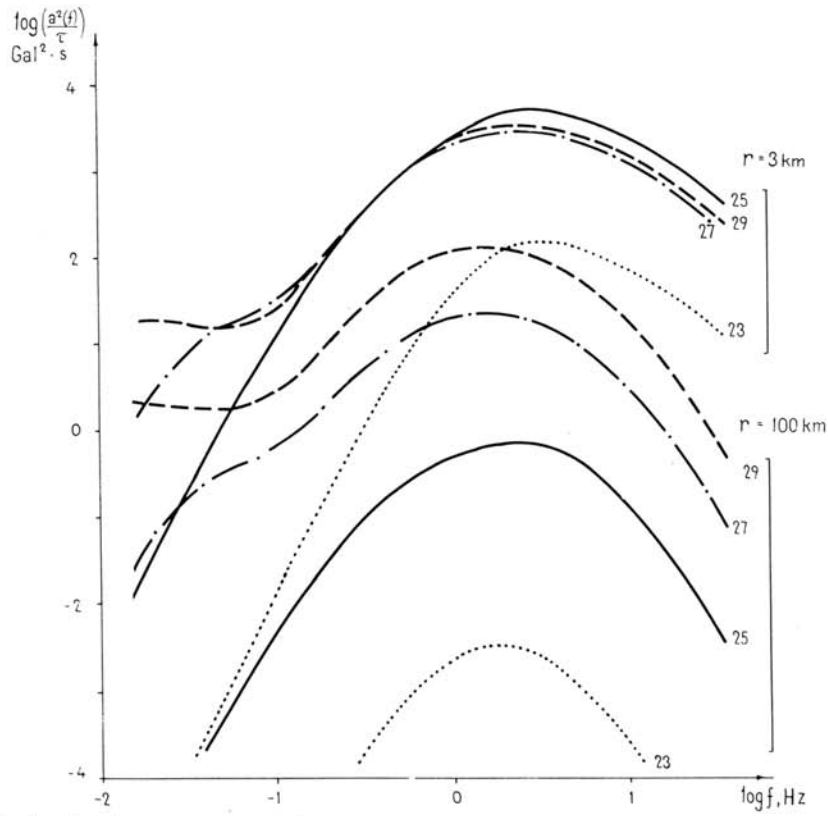

Figure 6. Acceleration power spectra for boxcar envelope approximation, with duration τ_{eff} and maximum envelope level preserved. Curves are plotted for $\log M_0 = 23$, 25, 27 and 29 ($M_{\text{LH}} = 4.20$, 6.11, 7.55 and 8.32, correspondingly) for distances 3 km ($\tau_{\text{eff}} = 0.55$, 2.2, 10 and 46 s) and 100 km ($\tau_{\text{eff}} = 8.0$, 8.3, 12.6 and 50 s).

A factor before $\log \tau_{\text{eff}}$ was accepted after reinterpretation of data collected by Aptikaev (1976) (in the original paper I was related to τ and not to $\log \tau$). $I(M)$ curves for the same set of r values are shown in Fig. 5, the value which gave the best fit with the empirical relation $I = 1.5M - 3.5 \log r + 3.0$ (Shebalin 1976) was accepted as the constant; this relation is also plotted. The upper limits $I_0 = I_0(M)$ are plotted according to the same paper. The overall agreement with data on $a_{\max}$ and I can be considered to be rather satisfactory.

Hanks (1979) proposed to characterize the near-field acceleration by its rms value a_{rms}. The more informative characteristic may be the power spectrum for an 'accelerogram' with effective duration and boxcar envelope. To illustrate this, such spectra were calculated for $r = 3$ and 100 km and $\log M_0 = 23$, 25, 27 and 29 (Fig. 6).

The accelerogram simulation programme was designed on the basis of the approach presented above. Its algorithm has recently been described briefly (Gusev & Fedotov 1980). In the simulation spectral shape, M_0, L, τ_{eff}, the envelope shape and impedance correction can be set independently, thus giving some additional opportunities for comparison with the presented simple estimates.

Discussion

A successful approximation of empirical relations $a_{\max}(M, r)$ and $I(M, r)$, on the basis of the approach we have presented, proves its validity, at any rate for rather large earthquakes, when the near-field short period radiation can be considered to be incoherent. This gives

some reason to our estimates for the fault surface. Being marginal, these estimates are rather interesting. Nevertheless, two important additional factors not accounted for earlier should be mentioned. Both must be pronounced in the immediate vicinity of the fault surface. Their effects are opposite and can compensate for one another. The first factor was mentioned before, it is a concentration of dislocation movement in the zone of rupture front, resulting in greater amplitudes. The second factor is a very strong wave attenuation in the fault zone (Q can be as low as 5). This factor is critical for 'sliding' rays and can markedly decrease the incoherent field amplitude. A static field contribution, when compared with the wavefield, is considerably lower, and its effects seem to be unessential as a rule.

It should be emphasized that the obtained estimates are only averages. The dispersion of values of G_{sp}, G, or a_{max} must be considerable, and it is difficult even to estimate their range now. A number of factors give rise to this dispersion: e.g. regional variations in spectral shape and level (variations of high-frequency 'cut-off' frequency in particular), directivity and stress drop variations. The role of focal mechanism should be mentioned specially. At moderate distances the wave propagation effects may be essential. P-wave contribution may be anomalously high at high frequencies because of tensile subsources. The study of these factors is a separate problem.

We used rather rough approximations in the course of our calculations. Exact expressions can easily be substituted in many cases, but we do not consider this to be useful at the present level of observational data.

Conclusion

The problem of describing short-period source radiation is important both for understanding the phenomen itself and for developing a technique for strong-motion simulation and prediction. Deterministic source models are inefficient for a wide-band description of source radiation, yet the statistical ones provide an adequate basis for such a description. Many difficulties arise, however, when we try to obtain numerical estimates of the model. Data of teleseismic wide-band observations are not very useful because of the nearly total absorption of short-period S while, near-field wide-band strong motion observations do not exist in practice. Another problem is the simultaneous inversion of wide-band records, which needs to combine rather different wave representations (surface waves, rays, scattered wavefield). These considerations led us to employ a simple indirect technique to obtain (at least preliminarily) estimates of the whole spectrum.

Equivalent point source radiation spectra obtained in the way described above are interesting and important; they cannot, however, be directly applied to estimate strong-motion parameters. The incoherent short-period radiation field of a finite source has its own specific regularities; corresponding theory is not absolutely new. Incoherent radiation fields arise, e.g. in noise acoustics and in lighting engineering. Several complications are produced by the effects of non-stationarity, wave scattering and a wide frequency band; however, no principle problems arise. Nevertheless, the process of generation and propagation of short-period radiation in individual earthquakes remains complicated even within the frame of our statistical approach. We need not know the source function in detail; but determination or prediction of the distribution of short-period radiation flux is itself a complicated problem. No clear way is seen now even for estimation of, e.g. f_1, f_2 and average G_{sp} for some individual future earthquake (e.g. the one filling the known 'seismic gap'). We believe, however, that our work provides not only a description, but also a useful conceptual framework for the prediction of strong motions from a large earthquake.

Acknowledgments

The author is indebted to Professor S. A. Fedotov for encouragement, to Drs N. V. Shebalin, V. V. Steinberg, T. G. Rautian, D. J. Andrews and V. M. Pavlov for helpful discussions, and to Drs J. Koyama and D. J. Andrews for sending their preprints.

References

Aki, K., 1967. Scaling law of seismic spectrum, *J. geophys. Res.*, **72**, 1217–1231.

Aki, K., 1972. Scaling law of earthquake source time-function, *Geophys. J. R. astr. Soc.*, **31**, 3–25.

Aki, K. & Chouet, B., 1975. Origin of coda waves: source, attenuation and scattering effects, *J. geophys. Res.*, **80**, 3322–3342.

Andrews, D. J., 1980. A stochastic source model. 1. Static case, *J. geophys. Res.*, **85**, 3867–3877.

Andrews, D. J., 1981. A stochastic source model. 2. Time-dependent case, *preprint.*

Aptikaev, F. F., 1976. The role of vibration duration by instrumental intensity estimation, in *Seismic Scale and Methods of Seismic Intensity Measurement*, pp. 234–239, Nauka, Moscow (in Russian).

Aptikaev, F. F. & Kopnichev, Yu. F., 1979. The role of focal mechanism by strong motion parameters prediction, *Dokl. Akad. Nauk. SSSR*, **247**, 822–825 (in Russian).

Blandford, A. A., 1975. A source model for complex earthquakes, *Bull. seism. Soc. Am.*, **65**, 1385–1405.

Boatwright, J. 1982. A dynamic model for far field acceleration, *Proc. XVI Workshop 'The dynamic characteristics of faulting inferred from recording of strong ground motion'*, pp. 213–238, Menlo Park.

Boore, D. M. & Joyner, M. B., 1978. The influence of rupture incoherence on seismic directivity, *Bull. seism. Soc. Am.*, **68**, 283–300.

Boore, D. M., Joyner, W. B., Oliver, A. A. & Page, R. A., 1980. Peak acceleration, velocity and displacement from strong motion records, *Bull. seism. Soc. Am.*, **70**, 305–321.

Burridge, R. & Halliday, G. S., 1971. Dynamic shear crack with friction as model for shallow-focus earthquakes, *Geophys. J. R. astr. Soc.*, **25**, 261–283.

Chouet, B., Aki, K. & Tsujiura, M., 1978. Regional variations of the scaling law of earthquake source spectra, *Bull. seism. Soc. Am.*, **68**, 49–79.

Dahlen, F. A., 1974. The ratio of *P*-wave to *S*-wave corner frequencies for shallow earthquake sources, *Bull. seism. Soc. Am.*, **64**, 1159–1180.

Das, S. & Aki, K., 1977a. A numerical study of two-dimensional spontaneous rupture propagation, *Geophys. J. R. astr. Soc.*, **50**, 643–668.

Das, S. & Aki, K., 1977b. Fault plane with barriers – a versatile earthquake model, *J. geophys. Res.*, **82**, 5658–5670.

Donovan, N. C., 1973. A statistical evaluation of strong ground motion data including the Feb. 9, 1971 San Fernando earthquake, *Proc. 5th World Conf. Earthquake Engineering*, **1**, 1252–1261, Rome.

Fedorova, I. V., Vandysheva, N. V., Golenetskaya, I. G., Gevondyan, V. B., Darechkina, N. M., Lazareva, A. P., Matorina, T. V., Medvedeva, G. Ya., Oborina, S. F., Skuinsh, P. A., Sinelnikova, L. G., Silina, I. K., Fabritsius, Z. E., Ferchev, M. D. & Chermnykh, G. P., 1974. Analysis of *P*-wave records at ESSN stations in relation with magnitude determination, in *Magnitude and Energy Classification of Earthquakes*, **1**, pp. 154–162, Nauka, Moscow (in Russian).

Geller, R. J., 1976. Scaling relations for earthquake source parameters and magnitudes, *Bull. seism. Soc. Am.*, **66**, 1501–1523.

Gumbel, E., 1965. *Statistics of Extremal Values*, Mir, Moscow, 450 pp. (in Russian).

Gusev, A. A., 1979. A descriptive statistical model for short period radiation from earthquake source, *Dokl. Akad. Nauk. SSSR*, **244**, 544–548 (in Russian).

Gusev, A. A. & Fedotov, S. A., 1980. Short-period seismic radiation and estimation of strong motion for large earthquake, *Proc. 7th World Conf. Earthquake Engineering*, Istanbul.

Hanks, T. C., 1979. b values and $\omega^{-\gamma}$ seismic source models: implications for tectonic stress variations along active crustal fault zones and the estimation of high-frequency strong ground motion, *J. geophys. Res.*, **84**, 2235–2242.

Haskell, N. A., 1964. Total energy and energy spectral density of elastic wave radiation from propagating faults, *Bull. seism. Soc. Am.*, **54**, 1811–1841.

Haskell, N. A., 1966. Total energy and energy spectral density of elastic wave radiation from propagating faults. 2. A statistical source model, *Bull. seism. Soc. Am.*, **56**, 125–140.

Housner, G. W., 1955. Properties of strong ground motion earthquakes, *Bull. seism. Soc. Am.*, **45**, 197–218.

Kanamori, H. & Anderson, D. L., 1975. Theoretical basis for some empirical relations in seismology, *Bull. seism. Soc. Am.*, **65**, 1073–1096.

Khalturin, V. I., 1974. Magnitude correlations expected and observed, in *Magnitude and Energy Classification of Earthquakes*, **1**, pp. 145–153, Nauka, Moscow (in Russian).

Kondorskaya, N. V., Gorbunova, I. V. & Landyreva, N. S., 1974. Magnitudes M_S and m_{PV} according to data of ESSN, NEIC and ISC, in *Magnitude and Energy Classification of Earthquakes*, 1, pp. 135–144, Nauka, Moscow (in Russian).

Kopnichev, Yu. F., Nersesov, I. L. & Medvedeva, E. V., 1980. Incoherent radiation of large earthquakes with different focal mechanisms, *Izv. Akad. Nauk. SSSR, Fizika Zemli*, No. 6, 14–25 (in Russian).

Kopnichev, Yu. F., Shpilker, G. L., 1978. Parameters of high-frequency radiation of earthquake source and a model for strong motion, *Dokl. Akad. Nauk. SSSR*, **239**, 193–196 (in Russian).

Kostrov, B. V., 1964. Self-similar problems of propagating shear rupture, *Appl. Math. Mech.*, **28**, 889–898 (in Russian).

Kostrov, B. V., 1966. Unsteady propagation of longitudinal shear crack, *Appl. Math. Mech.*, **30**, 1042–1049 (in Russian).

Koyama, J., Takemura, M. & Suzuki, Z., 1980. A scaling model for quantification of earthquakes in and near Japan, *preprint*.

Mikumo, T. & Miyatake, T., 1978. Dynamical rupture process on a 3D fault with non-uniform frictions, and near-field seismic waves, *Geophys. J. R. astr. Soc.*, **54**, 417–438.

Nur, A., 1978. Non-uniform friction as a physical basis for earthquake mechanics, *Pure appl. Geophys.*, **116**, 964–989.

Page, R. A., Boore, D. M. & Dieterich, J. H., 1975. Estimation of bedrock motion at ground surface in studies for seismic zonation of the San-Francisco Bay Region, *Prof. US geol. Surv. Pap.*, **947-A**, A31–A38.

Papgeorgio, A. S. & Aki, A., 1982. A specific barrier model for the quantitative description of inhomogeneous faulting and the prediction of strong ground motion. I. Description of the model, *Proc. XVI Workshop 'The dynamic characteristics of faulting inferred from recording of strong ground motion'*, pp. 311–352, Menlo Park.

Rascon O. A. & Cornell, C. A., 1969. A physically based model to simulate strong earthquake records on firm ground, *Proc. 4th World Conf. Earthquake Engineering*, **1**, 84–86, Santiago, Chile.

Rautian, T. G., 1976. The roles of source function and medium response in the model of formation of seismic vibrations, in *Problems of Engineering Seismology*, iss. 18, pp. 3–14, Nauka, Moscow (in Russian).

Rautian, T. G., Khalturin, V. I., Martynov, V. G. & Molnar, P., 1978. Preliminary analysis of the spectral content of *P*- and *S*-waves from local earthquakes in the Garm, Tadgikistan region, *Bull. seism. Soc. Am.*, 68, 949–971.

Rautian, T. G., Khalturin, V. I. & Zakirov, M. S., 1980. Study of conditions in earthquake sources by means of seismic coda, in *Physical Processes in Earthquake Sources*, pp. 224–256, Nauka, Moscow (in Russian).

Rautian, T. G. & Nikiforova, M. M., 1980. Study of spectral and temporal properties of earthquakes near the dam of Nurek Hydro, in *Seismic Effect upon Hydrotechnical and Power Constructions*, pp. 144–158, Nauka, Moscow (in Russian).

Riznichenko, Yu. V. & Seiduzova, S. S., 1972. A system of average earthquake energy spectra, *Izv. Akad. SSSR, Nauk, Fizika Zemli, No. 11*, 3–7 (in Russian).

Seismic microzoning, 1977, Nauka, Moscow, p. 34 (in Russian).

Shebalin, N. V., 1971. Comments on dominating period, spectrum and source of large earthquake, in *Problems of Engineering Seismology*, iss. 15, pp. 50–78, Nauka, Moscow (in Russian).

Shebalin, N. V., 1974. *Large Earthquake Sources on the Territory of the USSR*, 54 pp., Nauka, Moscow (in Russian).

Shebalin, N. V., 1976. On estimation of seismic intensity, in *Seismic Scale and Method of Measurement of Seismic Intensity*, pp. 87–109, Nauka, Moscow (in Russian).

Shnabel, P. B. & Seed, H. B., 1973. Accelerations in rock for earthquakes in the Western United States, *Bull. seism. Soc. Am.*, **63**, 501–516.

Sibson, R. H., 1977. Kinetic shear resistance, fluid pressure and radiation efficiency during seismic faulting, *Pure appl. Geophys.*, **115**, 387–400.

Stewart, G. S. & Kanamori, H., 1978. Complexity of rupture propagation in large earthquakes, *Trans. Am. Geophys. Un.*, **59**, 1127.

Thatcher, W. & Hanks, T. C., 1973. Source parameters of Southern California earthquakes, *J. geophys. Res.*, **78**, 8547–8576.

Trifunac, M. D., 1976a. Preliminary analysis of the peaks of strong earthquake ground motion, dependence of peaks on earthquake magnitude, epicentral distance and recording site conditions, *Bull. seism. Soc. Am.*, **66**, 189–219.

Trifunac, M. D., 1976b. Preliminary empirical model for scaling Fourier amplitude spectra of strong ground motion in terms of earthquake magnitude, source to station distance and recording site conditions, *Bull. seism. Soc. Am.*, **66**, 1343–1373.

Trifunac, M. D. & Brady, A. G., 1975. On the duration of strong earthquake ground motion, *Bull. seism. Soc. Am.*, **65**, 581–626.

Vostrikov, G. A., 1973. Size distribution of earthquake generating faults and some consequences, *Izv. Akad. Nauk. SSSR, Fizika Zemli, No. 12*, 32–49 (in Russian).

Zapolskii, K. K., Zhbrykunova, N. A., Zhbrykunov, V. Ya. & Loginova, G. M., 1973. Spectral content of *P*-waves from large earthquakes, in *Earthquakes in the USSR in 1969*, pp. 220–227 (in Russian).

Zhbrykunova, N. A. & Zhbrykunov, V. Ya., 1974. On a maximum magnitude in *P*-wave ChISS spectrum, in *Magnitude and Energy Classification of Earthquakes*, **1**, 198–206, Nauka, Moscow (in Russian).